Supplementary Information for

Silicon disulfide for high-performance Li-ion batteries and solid-state electrolytes

*Ki-Hun Nam,[a,b] Do-Hyeon Kim,[a,b] Young-Han Lee,[a,b] Su Cheol Han,[c] Jeong-Hee Choi,[c,d] Yoon-Cheol Ha[*c], and Cheol-Min Park[*a,b]*

[a] *School of Materials Science and Engineering, Kumoh National Institute of Technology, Gumi, Gyeongbuk, 39177, Republic of Korea*

[b] *Department of Energy Engineering Convergence, Kumoh National Institute of Technology, Gumi, Gyeongbuk, 39177, Republic of Koreac*

[c] *Next Generation Battery Research Center, Korea Electrotechnology Research Institute (KERI), 12 Jeongiui-gil, Seongsan-gu, Changwon-si, Gyeongsangnam-do, 51543, Republic of Korea*

[d] *Electro-Functionality Materials Engineering, University of Science and Technology (UST), 217 Gajeong-ro, Yuseong-gu, Daejeon, 34113, Republic of Korea*

**Corresponding author*
E-mail: cmpark@kumoh.ac.kr (C.-M. Park), ycha@keri.re.kr (Y.-C. Ha)

1. Si–S phase diagram

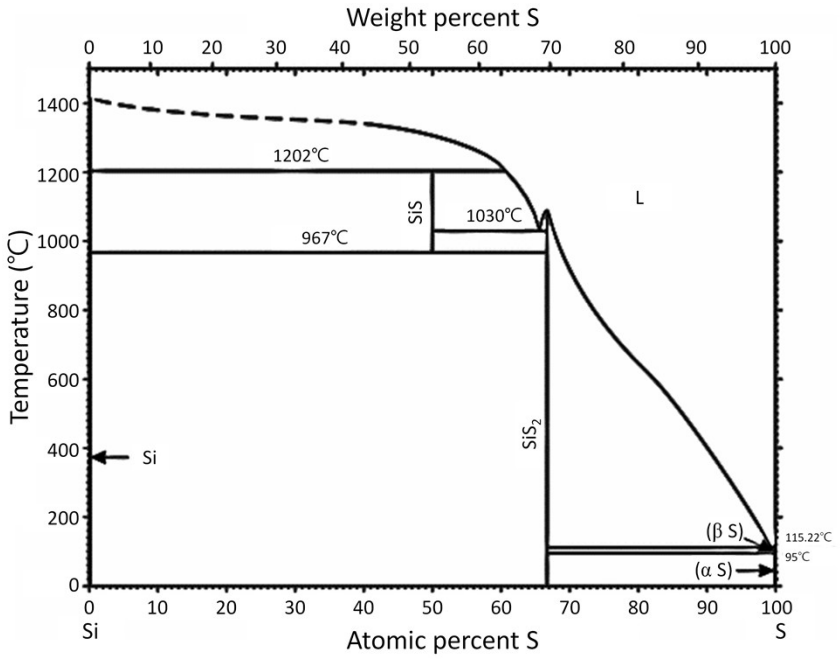

Fig. S1 Si–S phase diagram.

2. Characteristics of bulk Si

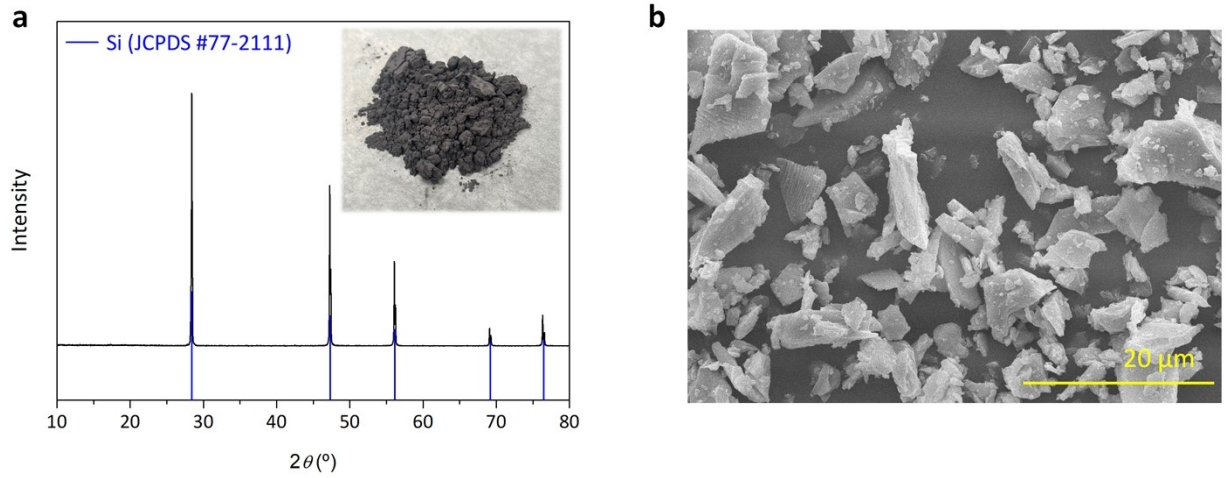

Fig. S2 Characteristics of bulk Si powder. (a) XRD pattern with color photo image and (b) SEM image of bulk Si.

3. Characteristics of bulk S

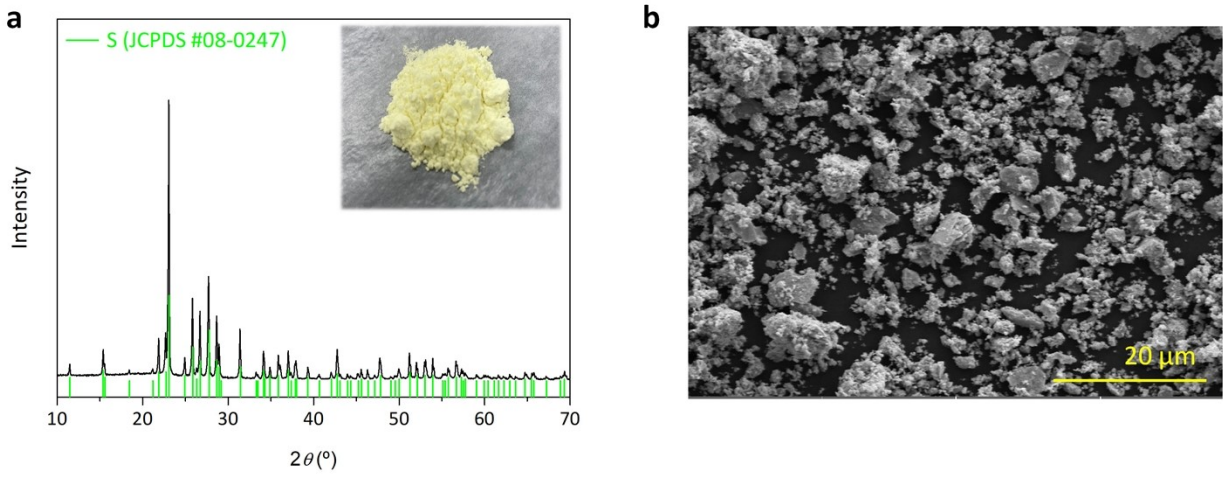

Fig. S3 Characteristics of bulk S powder. (a) XRD pattern with color photo image and (b) SEM image of bulk S.

4. Electrochemical performance of bulk Si

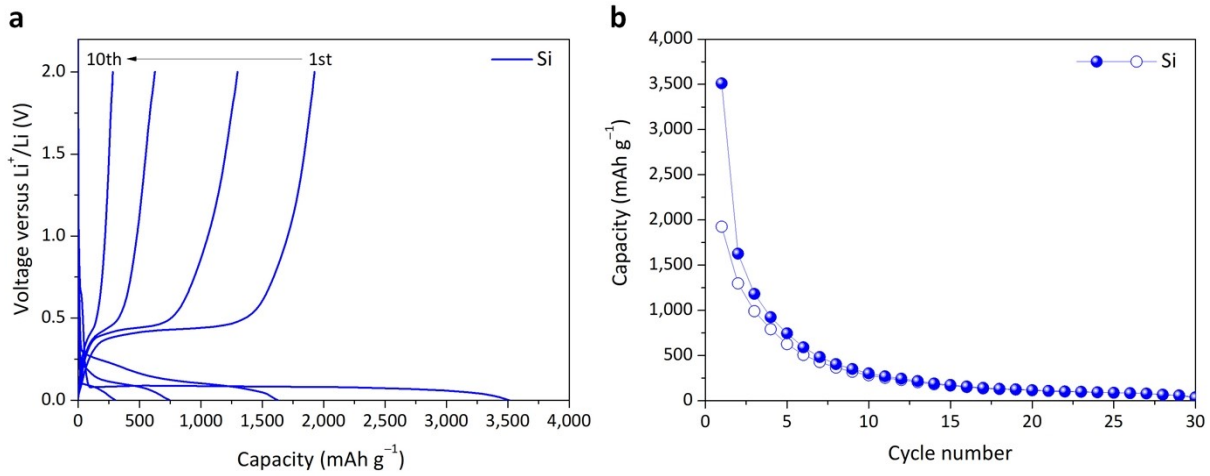

Fig. S4 Electrochemical performance of bulk Si. (a) GDC profiles (current density: 0.1 A g^{-1}) and (b) cycling performance of Si anode (cycling rate: 0.1 A g^{-1}).

5. Electrochemical performance of bulk S

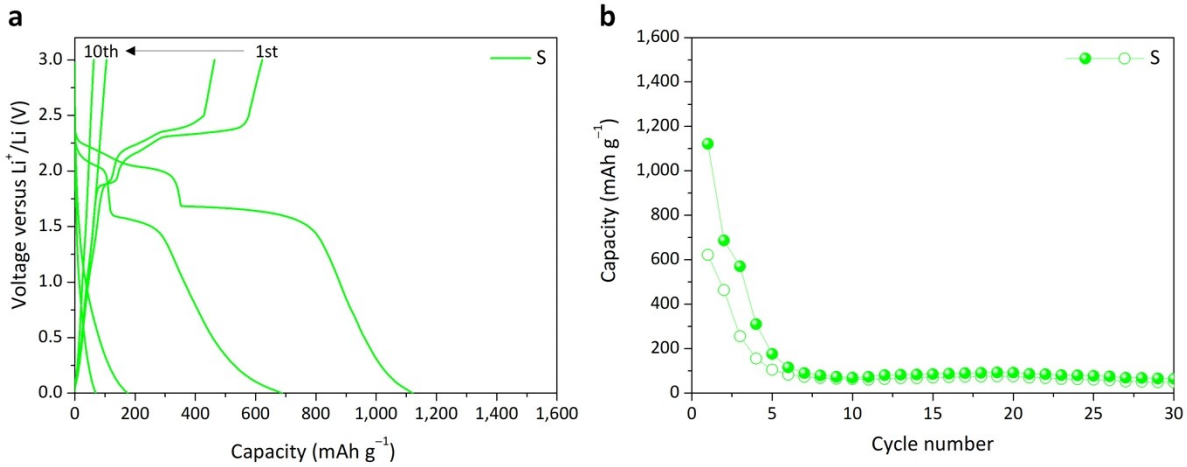

Fig. S5 Electrochemical performance of bulk S. (a) GDC profiles (current density: 0.1 A g^{-1}) and (b) cycling performance of S anode (cycling rate: 0.1 A g^{-1}).

6. *Ex-situ* XRD patterns of SiS_2 anode during first lithiation/delithiation cycle

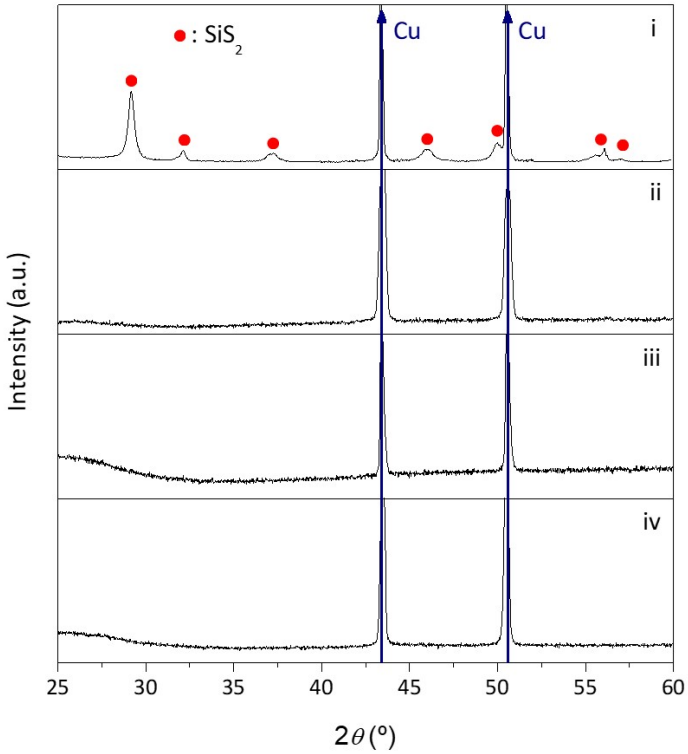

Fig. S6 *Ex-situ* XRD patterns of SiS_2 anode during first lithiation/delithiation. i) open circuit voltage, ii) lithiated 1.5 V, iii) fully lithiated 0 V, and iv) fully delithiated 3 V.

7. *Ex-situ* Raman spectra of SiS_2 anode during first lithiation/delithiation cycle

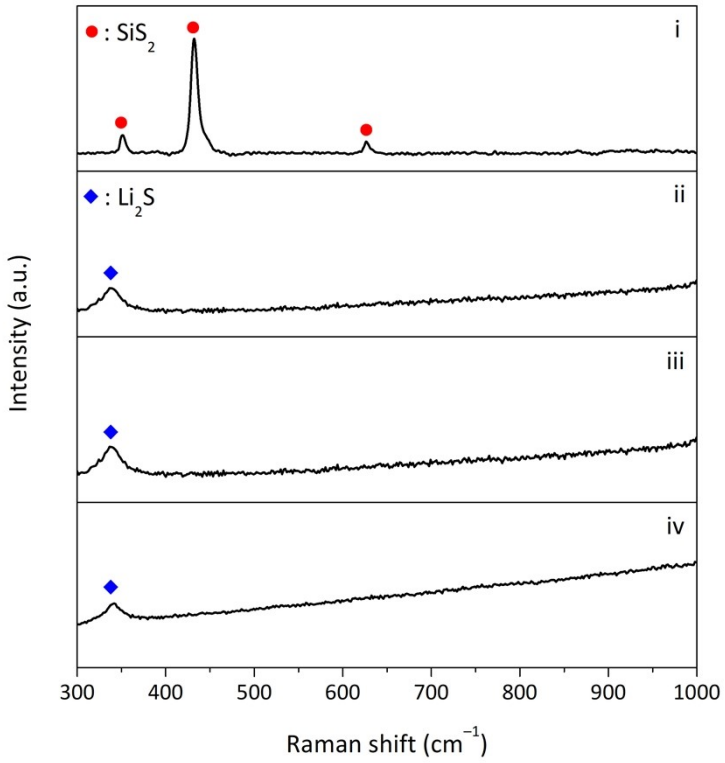

Fig. S7 *Ex-situ* Raman spectra of SiS_2 anode during first lithiation/delithiation cycle. i) open circuit voltage, ii) lithiated 1.5 V, iii) fully lithiated 0 V, and iv) fully delithiated 3 V.

8. Characteristics of SiS_2 nanocomposite

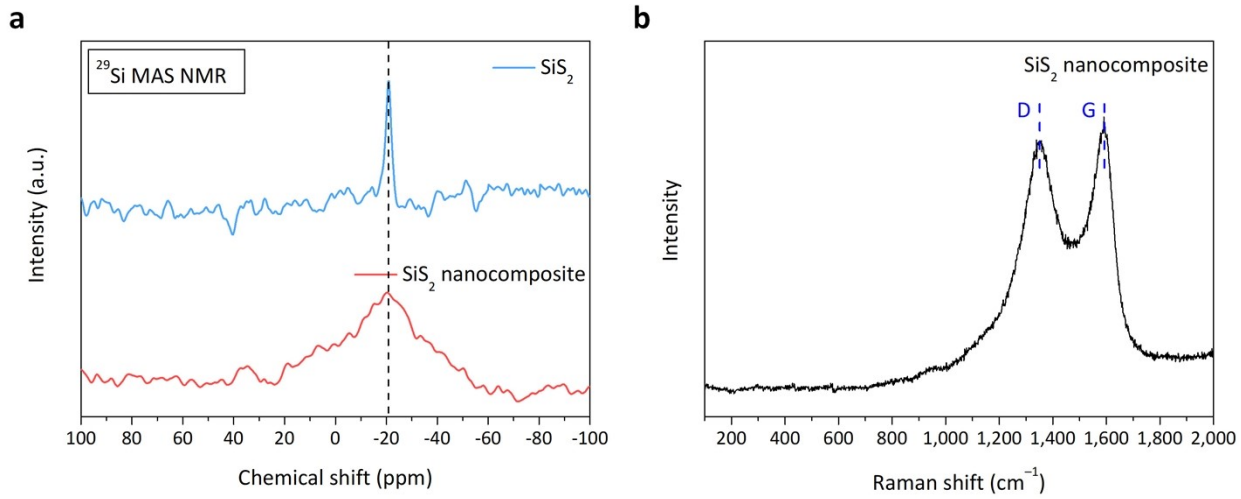

Fig. S8 Characteristics of SiS_2 nanocomposite. (a) Solid-state ^{29}Si NMR spectra of SiS_2 and SiS_2 nanocomposite. (b) Raman spectrum of SiS_2 nanocomposite.

9. Morphological characteristics of SiS_2 nanocomposite

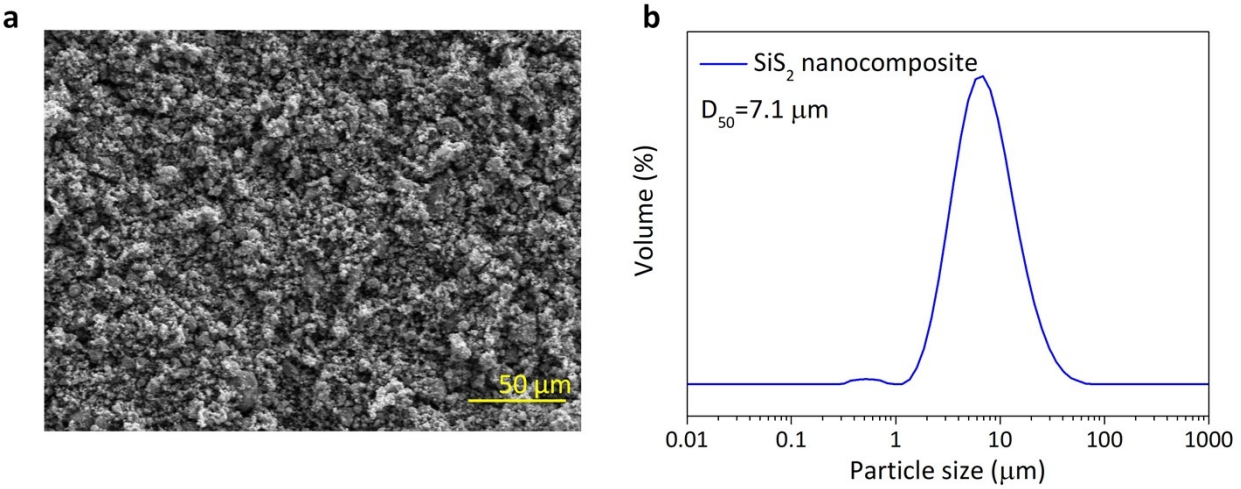

Fig. S9 Morphological characteristics of the SiS_2 nanocomposite. (a) SEM image and (b) PSA result of the SiS_2 nanocomposite.

10. Electrochemical impedance results of SiS_2 nanocomposite

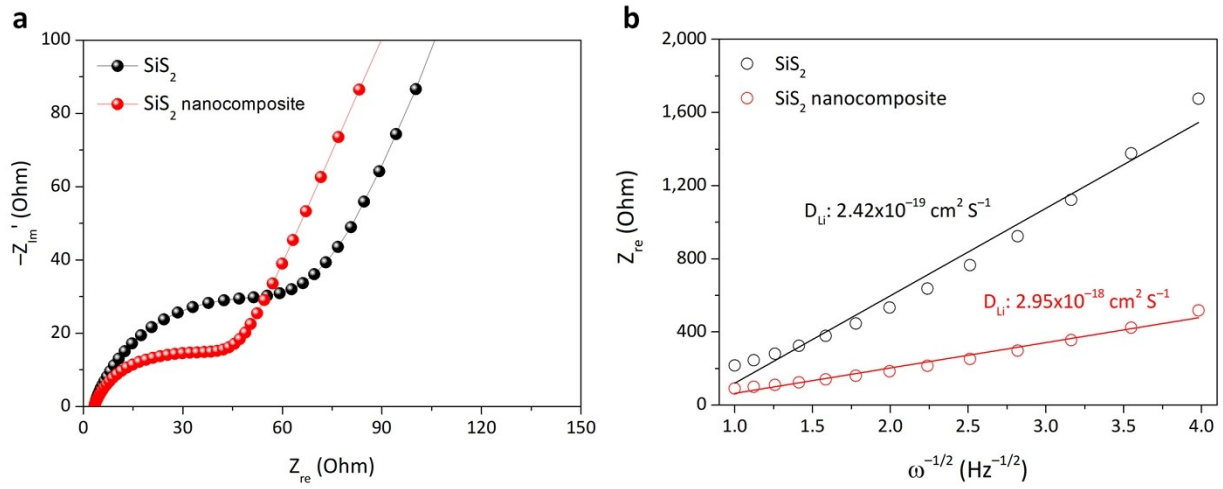

Fig. S10 Electrochemical impedance results of SiS_2 and SiS_2 nanocomposite anodes. (a) Nyquist plots of SiS_2 and SiS_2 nanocomposite anodes. (b) Linear relationship between Z_{re} and angular frequency ($\omega^{-1/2}$) of SiS_2 and SiS_2 nanocomposite anodes in low-frequency range.

11. dQ/dV results of SiS_2 nanocomposite

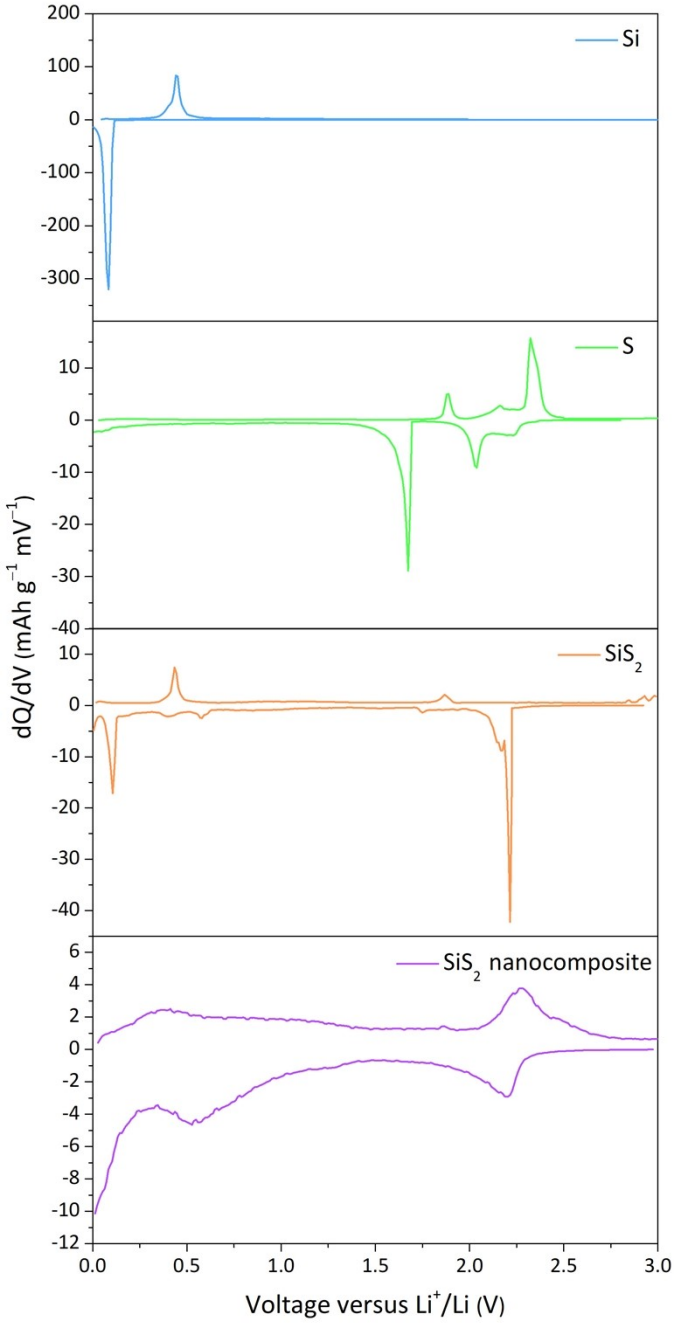

Fig. S11 dQ/dV plots of Si, S, SiS_2, and SiS_2 nanocomposite anodes. First-cycle dQ/dV plot results of Si, S, SiS_2, and SiS_2 nanocomposite anodes.

12. Characteristics and electrochemical performance of ball-milled carbon black

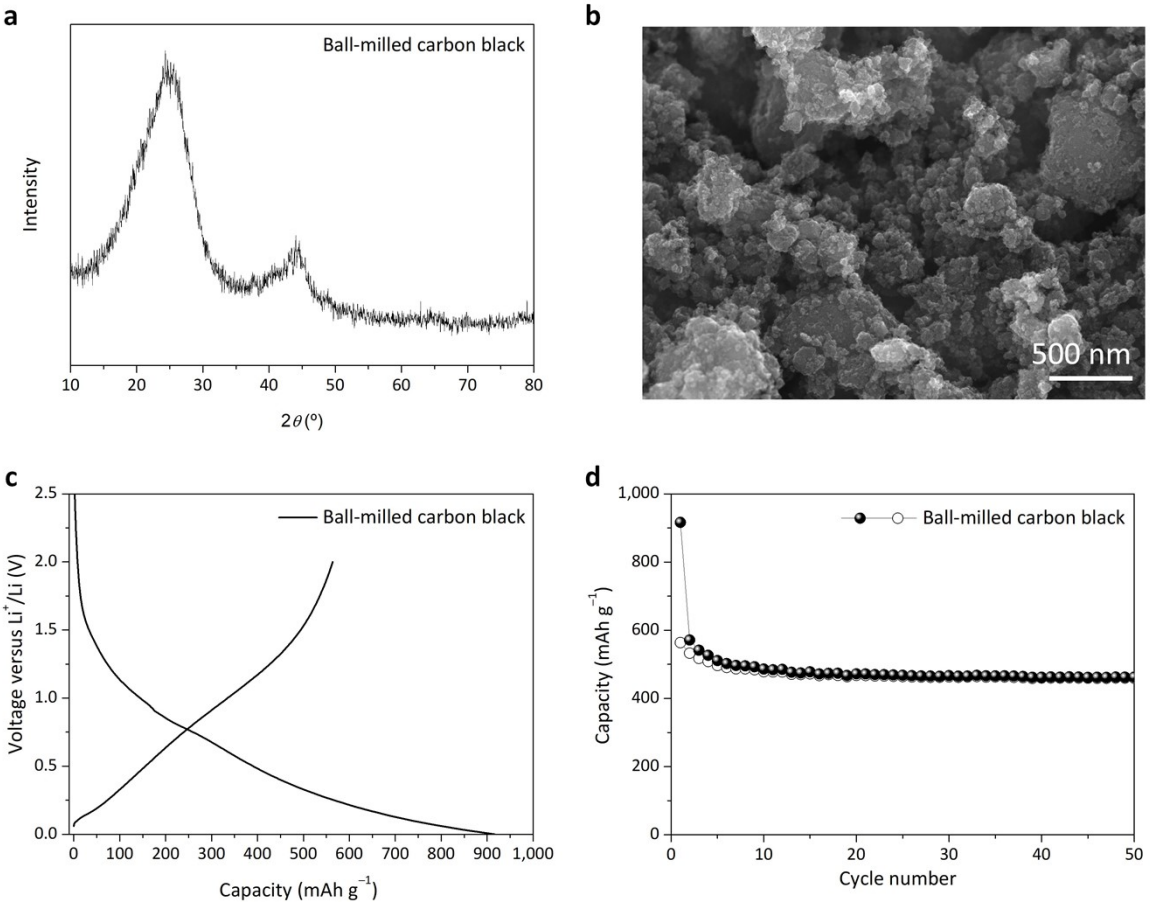

Fig. S12 Characteristics and electrochemical performance of ball-milled carbon black. (a) XRD pattern, (b) SEM image, (c) GDC profiles (current density: 0.1 A g^{-1}), and (d) cycling performance (cycling rate: 0.1 A g^{-1}) of ball-milled carbon black.

13 Electrochemical impedance results of SiS_2 nanocomposite after cycling

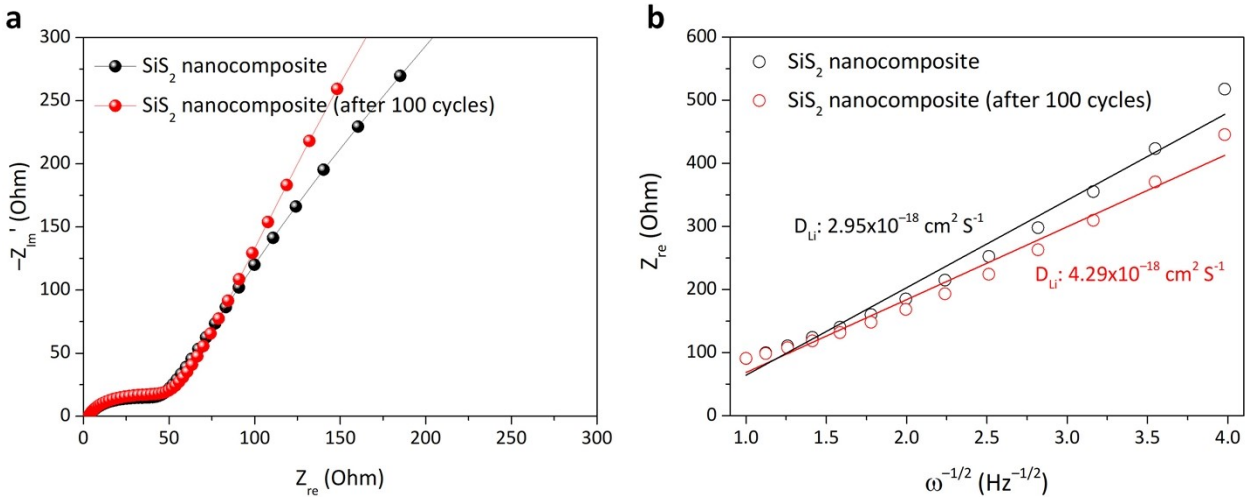

Fig. S13 Electrochemical impedance results of SiS_2 nanocomposite anodes after cycling. (a) Nyquist plots of SiS_2 nanocomposite anodes before and after 100 cycles and (b) corresponding linear relationship between Z_{re} and angular frequency ($\omega^{-1/2}$) in low-frequency range.

14. *Ex-situ* XPS of SiS_2 nanocomposite after cycling

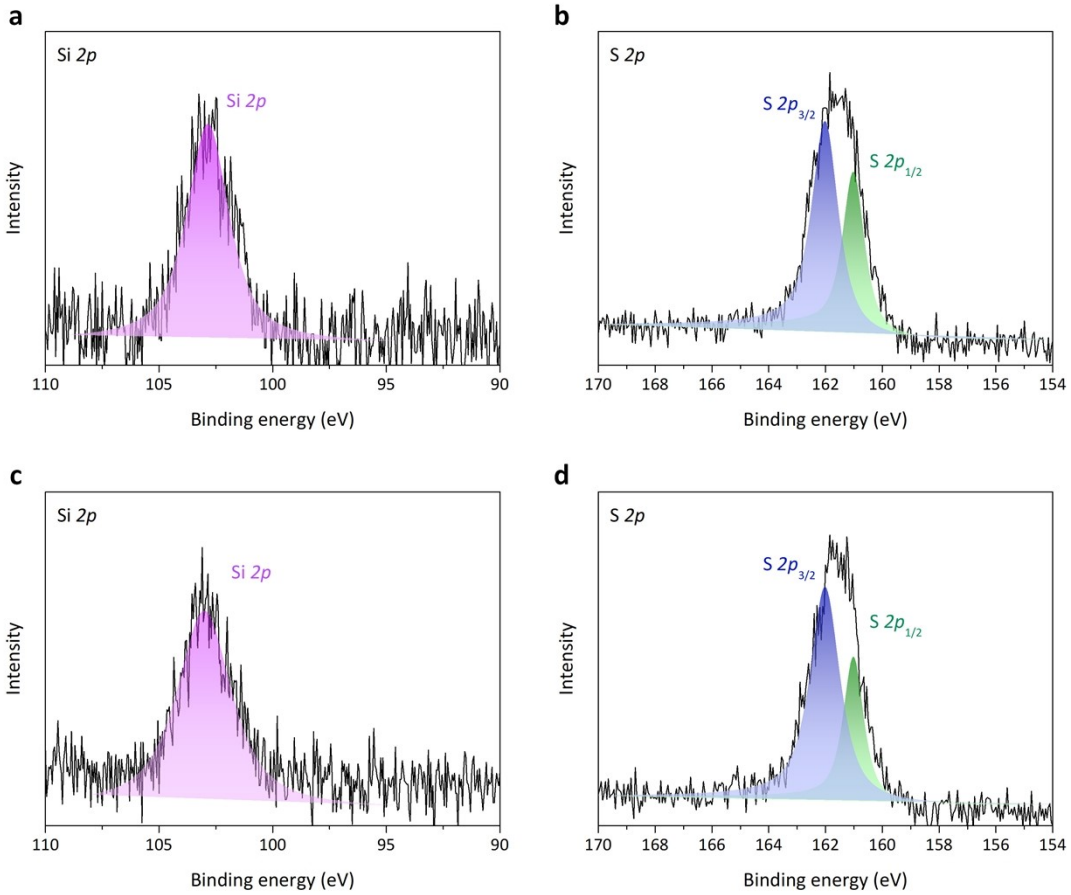

Fig. S14 *Ex-situ* XPS of SiS_2 nanocomposite anodes after cycling. (a) Si *2p* and (b) S *2p* XPS spectra of SiS_2 nanocomposite anode before cycle. (c) Si *2p* and (d) S *2p* XPS spectra of SiS_2 nanocomposite anode after 50 cycles.

15. XRD pattern of BM-$Li_{6.2}Si_{0.2}P_{0.8}S_5Cl$ synthesized using Li_2S, P_2S_5, LiCl, Si, and S precursors

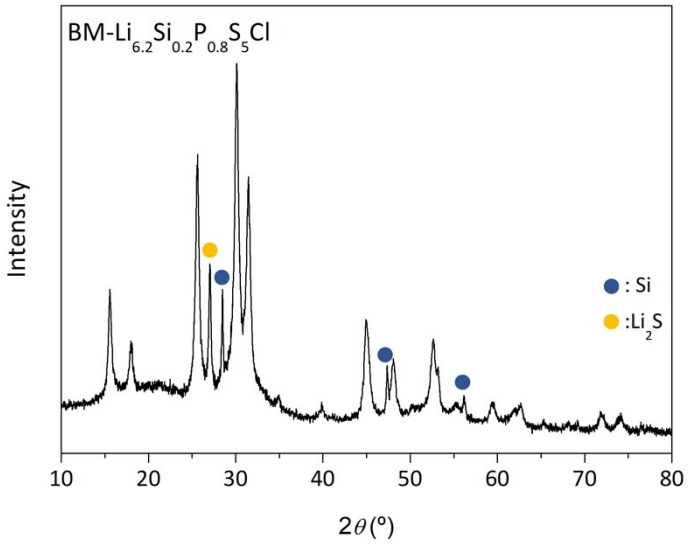

Fig. S15 XRD pattern of BM-$Li_{6.2}Si_{0.2}P_{0.8}S_5Cl$ (type 3) synthesized using Li_2S, P_2S_5, LiCl, Si, and S precursors.

16. HR-TEM images of HT-Li_6PS_5Cl and HT-$Li_{6.2}Si_{0.2}P_{0.8}S_5Cl$ SSEs

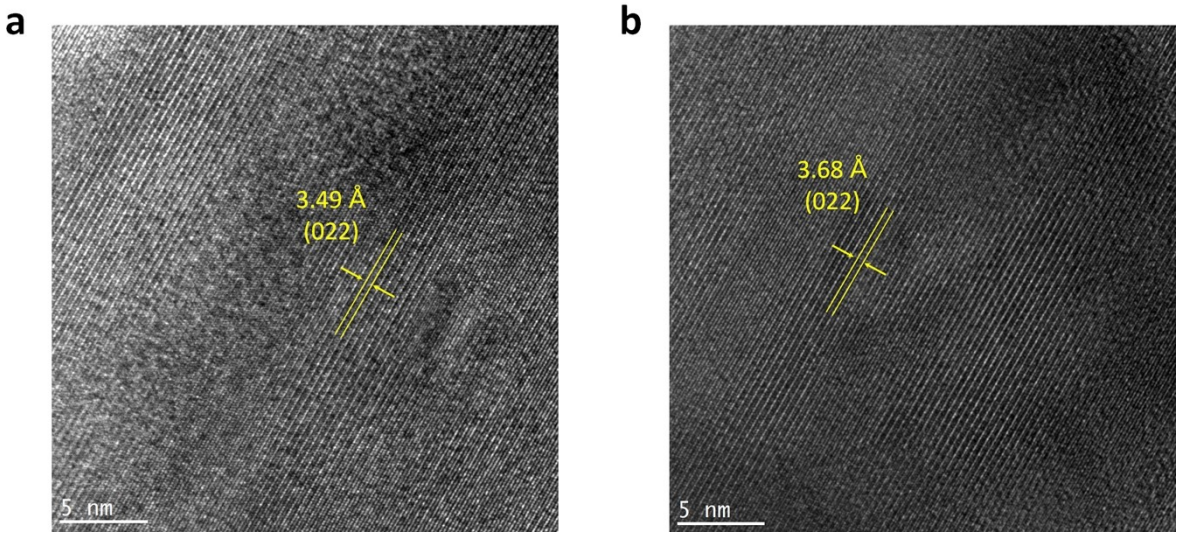

Fig. S16 HR-TEM images of (a) HT-Li_6PS_5Cl and (b) HT-$Li_{6.2}Si_{0.2}P_{0.8}S_5Cl$ SSEs.

17. Electrochemical performance of $Li_{0.5}In$/SSE/NCM622 full cells at 60 °C

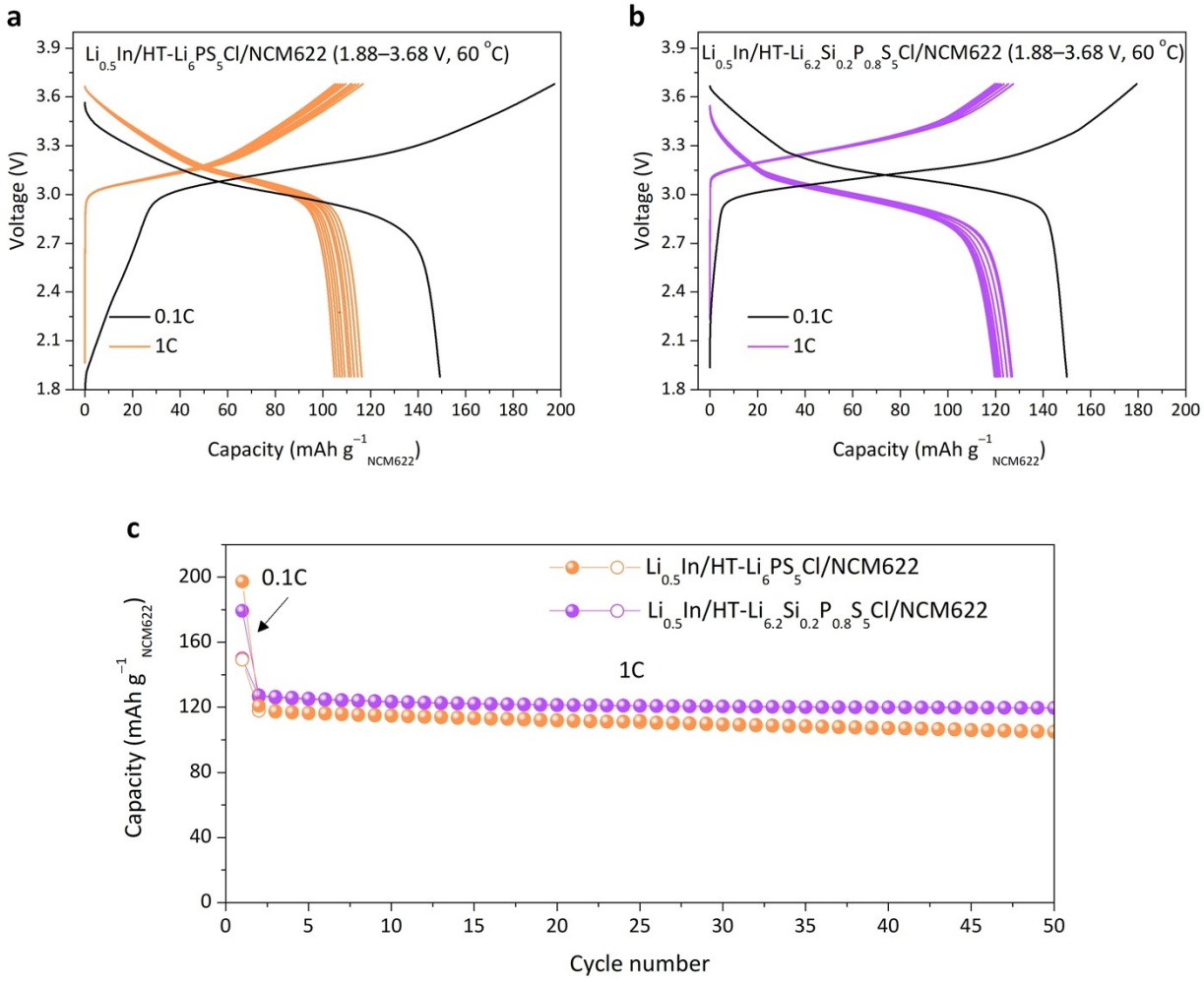

Fig. S17 Electrochemical performance of $Li_{0.5}In$/SSE/NCM622 full cells at 60 °C. Voltage profiles of (a) $Li_{0.5}In$/HT-Li_6PS_5Cl/NCM622 and (b) $Li_{0.5}In$/HT-$Li_{6.2}Si_{0.2}P_{0.8}S_5Cl$/NCM622/NCM622 full cells (1C = 160 mA g^{-1}). (c) Cycling performance of $Li_{0.5}In$/HT-Li_6PS_5Cl/NCM622 and $Li_{0.5}In$/HT-$Li_{6.2}Si_{0.2}P_{0.8}S_5Cl$/NCM622 full cells (1C = 160 mA g^{-1}).